Relative Surface Charge Density Mapping with the Atomic Force Microscope

William F. Heinz and Jan H. Hoh
Department of Physiology, Johns Hopkins University School of Medicine, Baltimore, Maryland 21205 USA

ABSTRACT An experimental approach for producing relative charge density maps of biological surfaces using the atomic force microscope is presented. This approach, called D minus D (D–D) mapping, uses isoforce surfaces collected at different salt concentrations to remove topography and isolate electrostatic contributions to the tip-sample interaction force. This approach is quantitative for surface potentials below 25 mV, and does not require prior knowledge of the cantilever spring constant, tip radius, or tip charge. In addition, D–D mapping does not require tip-sample contact. The performance of D–D mapping is demonstrated on surfaces of constant charge and varying topography (mechanically roughened mica and stacked bilayers of dipalmitolphosphatidylserine), a surface of varying charge and varying topography (patches of dipalmitolphosphatidylcholine on mica), and bacteriorhopsin membranes adsorbed to mica.

INTRODUCTION

Local electrostatic properties have a profound impact on the structure and function of biological systems. Ideally, both the amount and location of charge within a biological system could be measured with high resolution under physiological conditions. Many techniques exist for determining the average charged state of soluble molecules, such as electrophoretic, titration, electrokinetic, and redox potential measurements; however, relatively few experimental methods can determine the spatial distribution of charge on surfaces, such as membranes (McLaughlin, 1989; Cevc, 1990). Cationic ferritin can label negative charges on membranes and cell surfaces and be visualized with electron microscopy (Danon et al., 1972). In solution, local ionic currents are measured with the vibrating probe (Jaffe and Nuccitelli, 1974) and the scanning ion-conductance microscope (Hansma et al., 1989). Spectroscopy-based measurements of surface electrostatics in aqueous environments are based on the partitioning of potential-sensitive molecules between the solution and the membrane (Ehrenberg, 1986; Barthel et al., 1988; Castle and Hubbell, 1976). The tip of an atomic force microscope (AFM) (Binnig et al., 1986) is sensitive to electrostatic interactions with a sample surface in solution; it can therefore provide quantitative information about surface charge densities with high spatial resolution.

Quantitative electrostatic measurements with the AFM are based on forces produced from overlapping electrical double layers as a charged probe is brought near a charged sample surface. This paradigm was initially developed for other experimental approaches, and has been particularly well utilized with the surface forces apparatus (SFA). The SFA work has shown that the Derjaguin, Landau, Verwey, and Overbeek Theory (DLVO) can be used to relate force measurements to surface charge (Israelachvili and Adams, 1977; Pashley, 1981; Israelachvili, 1992). It has since been shown that DLVO theory can be applied to AFM measurements (Ducker et al., 1991). Subsequently, a number of groups have measured surface charge density and Debye length as a function of pH, electrolyte type, and concentration with the AFM and found agreement with standard DLVO theory for measurements over hard surfaces (Ducker et al., 1991, 1992; Butt, 1991a; Hillier et al., 1996; Larson et al., 1997; Raiteri et al., 1996a, b; Biggs and Proud, 1997). All these measurements are based on fitting force-distance curves to DLVO theory and thus require an absolute measurement of the tip-sample separation distance, D. Because current atomic force microscopes have no method independent of the tip-sample interaction to determine D, in practice force-distance curves have to include tip-sample contact.

The AFM has been used to map the spatial distribution of surface charge using arrays of force-distance curves or using isoforce images based on a repulsive double-layer force. Force distance (FD) curves have been used to examine the spatial distribution of charge on biological membranes (Butt, 1992). More recently, large arrays of force curves were used to examine charge distribution on positively charged amphiphilic bilayer patches (Rotsch and Radmacher, 1997) and biological membranes (Heinz and Hoh, 1997). These measurements fit force-curve data to DLVO theory and require tip-sample contact to obtain D. Double-layer based contact-mode imaging has been used to visualize charge contributions from silicon nitride surfaces (Senden et al., 1994), amphiphilic hemimicelles (Manne et al., 1994), and biological membranes (Müller and Engel, 1997) based on changes in apparent height of structures. These results qualitatively show that electrostatics contribute to AFM image contrast; any quantitative analysis requires additional topographic imaging and thus significant tip-sample contact.

Received for publication 11 May 1998 and in final form 10 September 1998.

Address reprint requests to Jan H. Hoh, Department of Physiology, Johns Hopkins University School of Medicine, 725 N. Wolfe Street, Baltimore, MD 21205. Tel.: 1-410-614-3795; Fax: 1-410-614-3797; E-mail: jan.hoh@jhu.edu.

0006-3495/99/01/528/11 $2.00

In this paper we present a quantitative analytical approach for determining relative surface charge density based on standard DLVO theory that does not require tip-sample contact. This approach uses isoforce surfaces collected at different salt concentrations to remove topographic contributions to force volumes, thus producing maps of relative charge density. The method does not require knowledge of the tip shape or charge density, both of which are difficult to obtain (and maintain). In addition, the approach is independent of the tip-sample contact point and can be used without the tip ever touching the sample, which reduces the risk of damaging the sample or contaminating the tip.

D–D MAPPING THEORY

Here we present a theoretical and analytical framework for determining relative charge densities from arrays of AFM force curves (i.e., force volumes) without the need for an absolute measurement of the tip-sample separation distance. This approach, called D minus D (D–D) mapping, is based on the classical electrical double-layer model and the Gouy-Chapmann theory, the electrostatic part of DLVO theory. The latter is a reasonable approximation for measurements beyond several nanometers, where van der Waals and hydration forces become small (Israelachvili and Adams, 1977; Pashley, 1981; Butt, 1991b; Israelachvili, 1992). The interaction force that arises from overlapping double layers when one charged surface (an AFM tip) is brought close enough to a second surface (e.g., biological membrane) is directly related to the charge density on, or the potential of, the two surfaces. While the two limits of the theory, constant charge and constant potential, diverge for small separations, they quickly converge at separations greater than several nanometers (Israelachvili, 1992). If we consider the AFM tip as a sphere and the sample as a flat plane, then the force, F, is described by

$$F(D) = \frac{4\pi R\lambda\sigma_R\sigma_S}{\epsilon} e^{-D/\lambda} \tag{1}$$

where R is the radius of the sphere, D the tip-sample separation distance, σ_R the surface charge density of the sphere, σ_S the surface charge density of the plane, ϵ the dielectric of the medium, and λ the Debye length (here we use 0.304 nm/$\sqrt{}$C for a monovalent ion of molar concentration C). Equation 1 holds so long as R, λ, σ_S, and σ_R do not vary significantly with D. We note that explicitly modeling the tip as an inverted pyramid instead of a sphere adds to Eq. 1 a geometrical factor independent of D that does not affect subsequent calculations (Butt, 1991b, 1992).

D–D mapping relates the relative surface charge distribution at different positions on a surface to the vertical (z axis) difference between two isoforce surfaces. First, consider the simplest case of two well-separated x-y positions (1 and 2) on a flat surface with two different charge densities (Fig. 1 *A*). Force curves are collected at each of these positions to a maximum force, F_{tr} (see Materials and Methods for a more detailed discussion of the trigger force), imposing the condition $F_1 = F_2 = F_{tr}$. When the charge densities at positions 1 and 2 are σ_1 and σ_2, respectively, and the measurement is performed in a monovalent salt solution with Debye length λ, this yields

$$\frac{4\pi R\lambda\sigma_R\sigma_1}{\epsilon} e^{-D_1/\lambda} = \frac{4\pi R\lambda\sigma_R\sigma_2}{\epsilon} e^{-D_2/\lambda}. \tag{2}$$

The ratio of surface charge densities is then easily found to be

$$\frac{\sigma_1}{\sigma_2} = e^{-(D_2-D_1)/\lambda}. \tag{3}$$

The relative surface charge of the sample can then be calculated from the difference (ΔD_{21}) in tip-sample separations, D_1 and D_2, provided the Debye length is known or is measured from the force curves.

To relate the relative charge densities to a measurable quantity that is independent of the absolute tip-sample separation distance, D, we begin by defining an isoforce surface, $Z_I = Z_I(x, y, F_{tr})$, that is the set of z-positions of the tip when it detects a force F_{tr} over a sample area (Fig. 1, *B* and *C*). Z_I is measured from the lowest point on the sample surface. Thus, the tip-sample separation distance at a given x-y position is found by subtracting the height, h, of a surface feature from the z-position of the isoforce surface, Z_I, which yields

$$D = Z_I - h, \tag{4}$$

and, by substitution into (3),

$$\frac{\sigma_1}{\sigma_2} = e^{-(Z_{I2}-h_2-Z_{I1}+h_1)/\lambda}. \tag{5}$$

Note that in practice Z_I is defined by the z-piezo's position, Z, relative to some arbitrary z-piezo position, Z_0. That is, $Z_I = Z + Z_0$. If this offset is the same at both positions (1 and 2), then Z_0 subtracts out of Eq. 5, and σ_1/σ_2 can be defined in terms of the z-piezo position:

$$\frac{\sigma_1}{\sigma_2} = e^{-(Z_2-h_2-Z_1+h_1)/\lambda}. \tag{6}$$

Equation 6 assumes and experimentally demands that the drift of either the cantilever or sample in the Z dimension is small between any adjacent pair of force curves. Note that if the sample is perfectly flat, h_1 and h_2 are zero, and Eq. 6 gives the relative charge densities. For samples with topography, the heights of the surface features need to be determined. This can be problematic for soft, sticky, easily deformable samples.

Our solution is to collect two isoforce surfaces in two electrolyte solutions and subtract one from the other, effectively removing the height information (Fig. 1, *D* and *E*). Consider force curves at positions 1 and 2 collected in low and high salt solutions that have Debye lengths λ_{low} and λ_{hi},

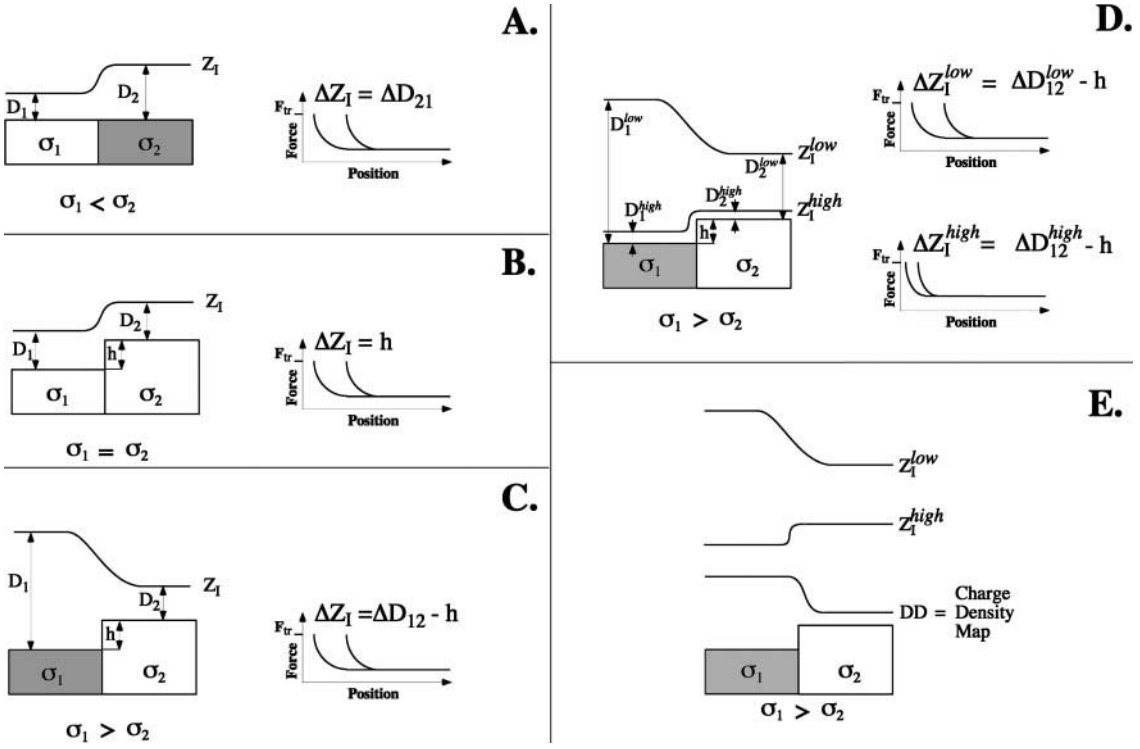

FIGURE 1 Schematic representation of samples with varying charge and topography, and the experimental and theoretical parameters used for D–D mapping. Samples are shown on the left side and force curves are shown on the right (except for *E*). (*A*) A sample with varying charge density and no topography. Force curves collected over the two regions are offset from each other in *z* due to the difference in charge. For a given force, F_{tr}, the difference in the *z*-position of the isoforce surface, $\Delta Z_I = \Delta D_{21} = D_2 - D_1$, is proportional to the natural log of the charge density ratio according to Eq. 3. The boundary between the two regions is broadened in the isoforce surface due to the finite extent of the tip and its double layer. (*B*) A sample with constant charge and varying topography. An isoforce surface, Z_I, measured over a sample with constant charge density and varying topography, has variations in its *z*-position due to the topographic variations only and not charge density differences. Applying Eq. 3 to this surface would result in an erroneous charge density ratio (which in this case is one). (*C*) A sample with varying charge and varying topography. The isoforce surface contains contributions from topography and charge. (*D*) Isoforce surfaces collected in low and high salt solutions over the sample in panel *C*. Both isoforce surfaces contain the same topographic contributions, but the electrostatic contributions are different (note the different amounts of broadening at the boundary). (*E*) Relationship between isoforce surface and D−D map. Because both isoforce surfaces contain the same height information, subtracting the high-salt surface from the low-salt surface yields a D–D surface that represents differences in surface charge density (Eq. 8).

respectively, then

$$\frac{\sigma_1}{\sigma_2} = e^{-(Z_2^{hi} - h_2 - Z_1^{hi} + h_1)/\lambda_{hi}} \quad \text{and} \quad \frac{\sigma_1}{\sigma_2} = e^{-(Z_2^{low} - h_2 - Z_1^{low} + h_1)/\lambda_{low}}. \tag{7}$$

Taking the natural logarithm and subtracting the equations yields

$$\ln\left(\frac{\sigma_1}{\sigma_2}\right) = \frac{[(Z_1^{low} - Z_2^{low}) - (Z_1^{hi} - Z_2^{hi})]}{\lambda_{low} - \lambda_{hi}}, \tag{8}$$

assuming that any variation in the true heights of the surface features due to salt changes are small compared to the changes in the isoforce surfaces. Equation 8 shows the ratio of surface charge densities, σ_1/σ_2, can be determined solely from the quantities *Z* and λ, which can be directly measured in a single experiment.

D–D mapping has several advantages over other AFM-based approaches for mapping surface charge density of soft samples. A relative measurement, it is independent of cantilever spring constant, exact tip size and surface charge density, and absolute *z*-position. All unknown factors, in this case *R* and σ_R, that do not vary with *D* cancel. Furthermore, because the Debye lengths are measured directly from the data, any two convenient electrolyte solutions can be used. Most importantly, this procedure is independent of the tip-sample contact point. The final map is a difference map, and if sufficiently low deflection trigger threshold (F_{tr}) is used the tip need not contact the surface at all. Lastly, absolute charge densities can be determined if an internal surface charge density standard is included at one of the positions.

MATERIALS AND METHODS

Sample preparation

Charged polystyrene spheres

Following Johnson and Lenhoff (1996), substrates were prepared by pipetting 100 μl polylysine (0.12 mg/ml in 20 mM NaCl, average mol wt 100; Sigma Chemical Co., St. Louis, MO) onto freshly cleaved 12-mm mica surfaces and allowing the polylysine to adsorb for 1 h before washing with buffer. Spheres functionalized with terminal carboxylic acid groups

(0.185, 2.22, and 9.1 COOH/nm^2, and 30, 120, and 160 nm diameter, respectively) obtained from Bangs Labs, Inc. (Fishers, IN) were diluted to volume fractions of 10^{-4} and 10^{-3} in pure (18.2 MΩ) water (2.22 COOH/nm^2) or 20 mM NaCl (0.185 and 9.1 COOH/nm^2). A 100 μl volume of the sphere solution was pipetted onto the polylysine-coated mica. Monolayer adsorption times varied by type of sphere from roughly 10 min (2.22 COOH/nm^2) to several hours (0.185 and 9.1 COOH/nm^2). Samples were washed gently with appropriate buffer, washed again in water, then air-dried overnight. Before use they were rehydrated with water.

Mechanically roughened mica

Mechanically roughened mica substrates were prepared by lightly sanding (one pass) a freshly cleaved mica disk with fine grit (600) sandpaper. The roughened mica was then washed under a stream of water for ~1 min and blow-dried with compressed air. Samples were immediately placed in the AFM for FV imaging.

Supported phospholipid bilayers

Supported lipid bilayers were prepared following the vesicle adsorption method (Fang and Yang, 1997; Tamm and McConnell, 1985). Briefly, dipalmitoylphosphatidylcholine (DPPC) and dipalmitoylphosphatidylserine (DPPS) (Avanti Polar Lipids, Alabaster, AL) were resuspended in 20 mM NaCl to a final concentration of 0.1 mg/ml and sonicated (70 W/55 kHz) for approximately 30 min. A 100-μl drop was then placed onto a freshly cleaved mica disk (for DPPC) or a polylysine-coated mica disk (for DPPS) and incubated for 2 h in a room-temperature humidor. After adsorption, the sample was incubated at 45°C for 20 min and then gently washed with ~3 ml of the NaCl solution to remove unabsorbed vesicles. Great care was taken not to expose the bilayer to air, in particular when mounting the sample in the AFM and during fluid exchange. Bilayers were stable for several weeks when kept hydrated and stored at 4°C.

Bacteriorhodopsin membranes

Following Butt (1992), bacteriorhodopsin (BR) membranes (Sigma) were diluted in water to roughly 5 mg/ml. They were then diluted 10–100-fold more into 100 mM K_2HPO_4 buffer, pH 9. A 50-μl volume was deposited onto mica substrates and allowed to adsorb for 30 min before a gentle wash with buffer to remove loosely bound membranes.

Atomic force microscopy

Instrumentation

A Nanoscope III or IIIa controller and a multimode atomic force microscope (Digital Instruments Inc., Santa Barbara, CA) equipped with a J-type scanner (maximum *x-y* scan range of ~150 × 150 μm with 5 μm vertical range) was used for all experiments. Imaging was performed using a standard fluid cell without the o-ring. Contact mode images of the samples were taken with a low imaging force (2–5 nN) and 1–4 Hz lateral scan rate. All forces reported are estimates based on the nominal spring constant values. It is important to note that calibration of the optical lever sensitivity before force measurements is essential to accurately convert the photodiode output voltage to cantilever deflection (D'Costa and Hoh, 1995).

Cantilevers

"V"-shaped silicon nitride cantilevers (Park Scientific Instruments, Sunnyvale, CA) were either 220 μm or 320 μm × 22 μm with nominal force constants of 0.03 and 0.01 N/m, respectively. For some experiments, the cantilevers were soaked for 15–30 min in 100 mM NaOH and then rinsed in a bath of 20–30 ml water for 30–60 min before use. Hydroxide treated tips sometimes have a greater surface charge density than untreated tips (unpublished data).

Force curves over charged-sphere monolayers

Individual force curves with *z*-displacements of 100–200 nm were collected at *z*-scan rates between 1 and 4 Hz (0.2–1.6 μm/s). Using a single cantilever for all samples, force curves were collected over the polystyrene sphere monolayers in solutions of various NaCl concentrations (0.2–100 mM). To ensure the position of the laser beam on the cantilever did not change appreciably when exchanging samples (i.e., become torqued by the surface tension), care was taken to maintain a large droplet around the cantilever. Ten curves were collected on each monolayer.

Force volumes for D–D mapping

Acquisition of force volume (FV) data sets, or force mapping, is supported by current versions (4.23 b6) of the Nanoscope control software (Support Note 240, Revision A, Digital Instruments). Force mapping involves the collection of force curves at each point in a regularly spaced array over a two-dimensional (2D) (*x-y*) scan area. This FV data set is a three-dimensional array of deflection values that are proportional to the *z*-components of the interaction force between the sample and the tip at specific *x-, y-, z*-positions over the sample. The D–D mapping approach requires that $F_1 = F_2 = F_{tr}$. To achieve this, the AFM was operated in relative trigger mode, that is, all force curves have the same preset maximum cantilever deflection (F_{tr}) relative to the cantilever's deflection at the beginning of the curve (zero deflection). Because we assume the cantilever is a simple spring and the deflection of the cantilever is proportional to the force, we use units of length and force interchangeably where appropriate. Also, current controlling software allows triggers on repulsive forces only; any attractive forces will cause the tip to jump to contact and push against the sample before triggering.

Force curves were collected by moving the piezo vertically until the cantilever deflection reached the trigger value, F_{tr}. The approach portion of the force curve is terminated at this point, and the piezo is retracted a predetermined distance (the *z*-scan size). The piezo's *z*-position at that deflection was recorded at that *x-y* position on the sample. This image will be referred to as the FV height image, or an isoforce surface (of force F_{tr}). This process was repeated for each point in the 2D (*x-y*) scan of the sample. Most of our measurements were 64 × 64 force curves over the area and each curve (approaching and retracting) was sampled 64 times. Some measurements were 32 × 32 force curves and 256 points per curve to obtain a higher vertical resolution in the force curves. These dimensions are an upper limit imposed by the current control software for our AFM.

For a D–D map, FV data sets over the same area were collected in high and low salt buffers (typically in the range 0.1–10 mM monovalent salt). Solutions were exchanged by gently drawing roughly 100 μl of solution out of the fluid cell with a pipette, then adding 100 μl of new solution to the cell. This was repeated several times to ensure complete exchange of solution. Fluid exchange was performed while the AFM was operating in FV mode. The relative trigger and the feedback loop prevented the tip from inadvertently hitting the sample.

For mapping relative surface charge density, it is crucial that the tip charge and radius remain constant throughout the entire measurement. To accomplish this, we set F_{tr} to a value low enough to ensure the tip never contacts the sample surface. This value was empirically determined, and trigger values of 5–15 nm (~0.05–0.45 nN) were used in all salt solutions.

Data analysis

Analysis of the force curves and the FV data sets was performed using a set of tools, developed in our laboratory using the Interactive Data Language (Research Systems, Inc., Boulder, CO) programming environment, called FCAP (Force Curve Analysis Program) and FVVR (Force Volume Visualization Routines). FCAP displays, modifies, and fits individual and

multiple force curves. The force curves were offset to remove cantilever drift and corrected to produce *FD* curves using the measured cantilever sensitivity. The curves were fit to Eq. 1 to extract charge density and Debye length. Similarly, FVVR offers numerous methods of displaying, modifying, and analyzing FV data. The D–D mapping approach has been automated in FVVR. Force curves from the FVs were fit to a simple decaying exponential to extract Debye lengths. Because Debye length is a function only of the bulk ionic strength, it should be uniform everywhere over the sample. Maps of Debye length are internal controls and verify that the measured forces reflect electrostatic interactions. The computations for a set of 4096 force curves take less than 60 s on a 225 MHz Macintosh-compatible computer. Because the piezo can drift laterally during the experiment, subtraction of the force volume isoforce surfaces was performed after aligning the images by eye. The D–D maps were then scaled to a suitable color table, such that lighter areas have a higher relative surface charge density.

RESULTS AND DISCUSSION

Forces vary with ionic strength and charge

The theory used in D–D predicts that force-distance curves collected with a charged tip over a charged surface in an aqueous solution will vary in predictable ways with the ionic concentration of the solution and the charge density of the sample. In the case of varying ionic concentration, the Debye length should decrease with increasing concentration, while the maximum repulsive force (for an interaction between like charges) achieved within several nanometers of contact should remain constant. In the case of varying charge the Debye length should remain constant while the maximum force should vary linearly (for surface potentials < 25 mV) with the charge density of the sample.

To verify these predictions in our experimental system, individual force curves were collected over monolayers of uniformly negative charged polystyrene and latex spheres with manufacturer-reported surface charge densities of 0.185, 2.22, and 9.1 COOH/nm^2 as determined by titration. Note that the degree ionization in each of these samples is not known, and thus the absolute surface charge density is unknown. For the experiments reported here, these spheres are only used as samples with increasing surface charge density. Representative force curves over a monolayer of 2.22 COOH/nm^2 spheres in three different NaCl concentrations are shown in Fig. 2 *A*. Notice that all curves have similar *y*-intercepts and different slopes. Averages of 10 curves give intercepts of 54 $\pm$ 3, 59 $\pm$ 5, and 39 $\pm$ 7 nm and slopes of 102 $\pm$ 5, 46 $\pm$ 4, and 18 $\pm$ 3 nm for low-, medium-, and high-ionic strength solutions, respectively. Fig. 2 *B* shows force curves collected over all three monolayers in solutions of roughly equal salt concentrations. Here, the slopes of the individual curves are nearly identical, but the intercepts differ. Averages of 10 curves give intercepts of 1.1 $\pm$ 1.4, 3.9 $\pm$ 0.7, and 37.9 $\pm$ 5.5 nm and slopes of 31 $\pm$ 3, 18 $\pm$ 3, and 14 $\pm$ 0.4 nm for spheres of 0.185, 2.22, and 9.1 COOH/nm^2, respectively. The variations in the Debye length in this case result from small variations in the concentration of the salt solution, which occur when samples are changed. Assuming complete ionization of all the titratable surface groups, the spheres would have surface charge densities, from least to greatest, of 0.185, 2.22, and 9.1 e$^-$/nm^2. These values represent the maximum possible surface charge densities. Thus the differences in the individual force curves measured over monolayers of these uniformly charged spheres demonstrate the AFM's ability to detect charge differences of less than a few e$^-$ per nm^2. These results show that the AFM behaves in a manner consistent with simple theory and that Eq. 1 is a reasonable description of the interaction between the tip and the sample.

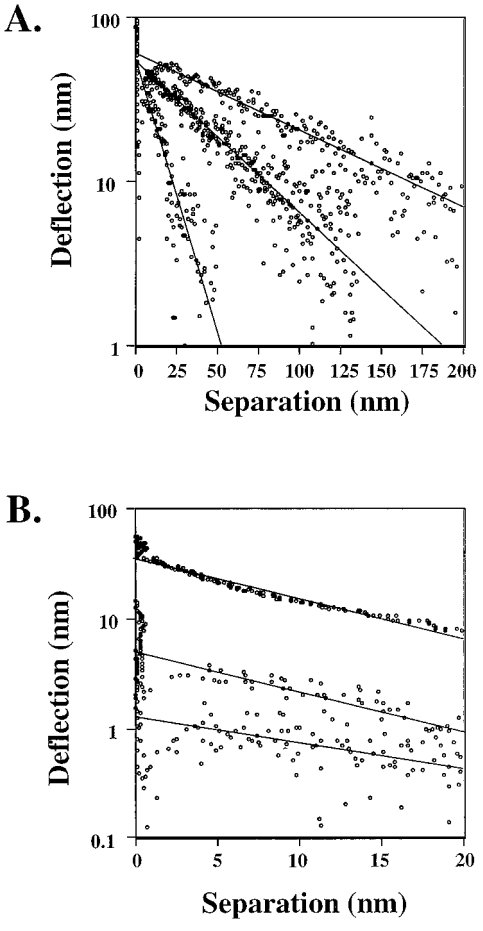

FIGURE 2 Force curves on polystyrene spheres with varying charge and at varying salt concentrations. (*A*) Individual force curves collected over a monolayer of charged polystyrene spheres (2.22 COOH/nm^2) in three different salt concentrations. The lines represent best fits to Eq. 1. From top to bottom, the intercepts are 57, 50, and 44 nm and the Debye lengths are 99, 52, and 16 nm. (*B*) Individual force curves collected over monolayers of spheres of three different charge densities (0.185, 2.22, and 9.1 COOH/nm^2) in a constant salt solution. The lines represent best fits to Eq. 1. From top to bottom, the intercepts are 34, 4.4, and 1 nm, and the Debye lengths are 29, 16, and 13 nm.

D–D map is a relative charge density map independent of topography

There are two limiting cases of D–D mapping: 1) surfaces that have a constant topography and varying charge density (Fig. 1 *A*); and 2) surfaces that have varying topography and

constant charge density (Fig. 1 *B*). The general case, a surface with variations in both charge density and topography (Fig. 1, *C* and *E*), falls between these limits. To show that D–D mapping can produce relative charge density maps that have small or no contributions from topography, we examined a mechanically roughened mica surface, and supported DPPS and DPPC lipid bilayers. The roughened mica and DPPS experiments correspond to the second case, and the DPPC experiment corresponds to the general case. The first case is not shown, because of the difficulty in producing a perfectly flat sample with regions of varying charge.

D–D map of surfaces with constant charge density and varying topography

We present two examples of D–D mapping of surfaces with varying topography and constant surface charge density. The first sample, mechanically roughened mica, has features whose height is greater than the Debye lengths ($h > \lambda$) and clearly shows the removal of topographic information from the D–D map. The second, stacked DPPS bilayers, has features whose height is similar to the Debye lengths ($h \simeq \lambda$).

Lightly sanding a freshly cleaved mica substrate results in gashes in the mica surface, with topographic steps of ~40 nm (Fig. 3, *A* and *E*) and a constant charge resulting from all solvent-exposed surfaces being negatively charged at neutral pH. The rough mica corresponds to the $h > \lambda$ case.

Force volumes collected over roughened mica in two different NaCl concentrations with $F_{tr} = 5$ nm reveal the underlying topography of the sample (Fig. 3, *B* and *C*). Debye length maps calculated from each force curve (Fig. 3, *F* and *G*) in the volumes (Debye lengths of 17 ± 2 and 7.4 ± 0.6 nm) are essentially flat, as would be predicted. When larger trigger forces are used, and an obvious hard contact is achieved, the Debye length maps are coupled to topography (data not shown). Thus they are an important control when isolating charge contributions from other sample properties. Subtracting the high salt isoforce surface (Fig. 3 *C*) from the low salt isoforce surface (Fig. 3 *B*) yields a constant, low contrast (flat) D–D map of the surface (Fig. 3 *D*) uncoupled from the topography (Fig. 3, *A* and *E*).

Because all features in this sample have equal surface charge densities, the electrostatic contribution to the isoforce surfaces is uniform (Fig. 1 *B*). Therefore the contrast in the high and low salt images is due to the topography of the sample. Line profiles (Fig. 3 *H*) along the high and low salt isoforce surfaces are essentially the same, and the difference map, therefore, is flat. These FV images and the resultant D–D map demonstrate that topographic contributions to the isoforce surfaces can be removed from the data, resulting, in this case, in a uniform map of relative surface charge density. The contrast on edges of the gash arises from three factors. Because the pixel size in these images is relatively large there is sometimes a problem in aligning the high-salt and low-salt isoforce surfaces. It is also possible that edges have a sufficiently different charge density to produce contrast. Finally, the effective radius of the probe is

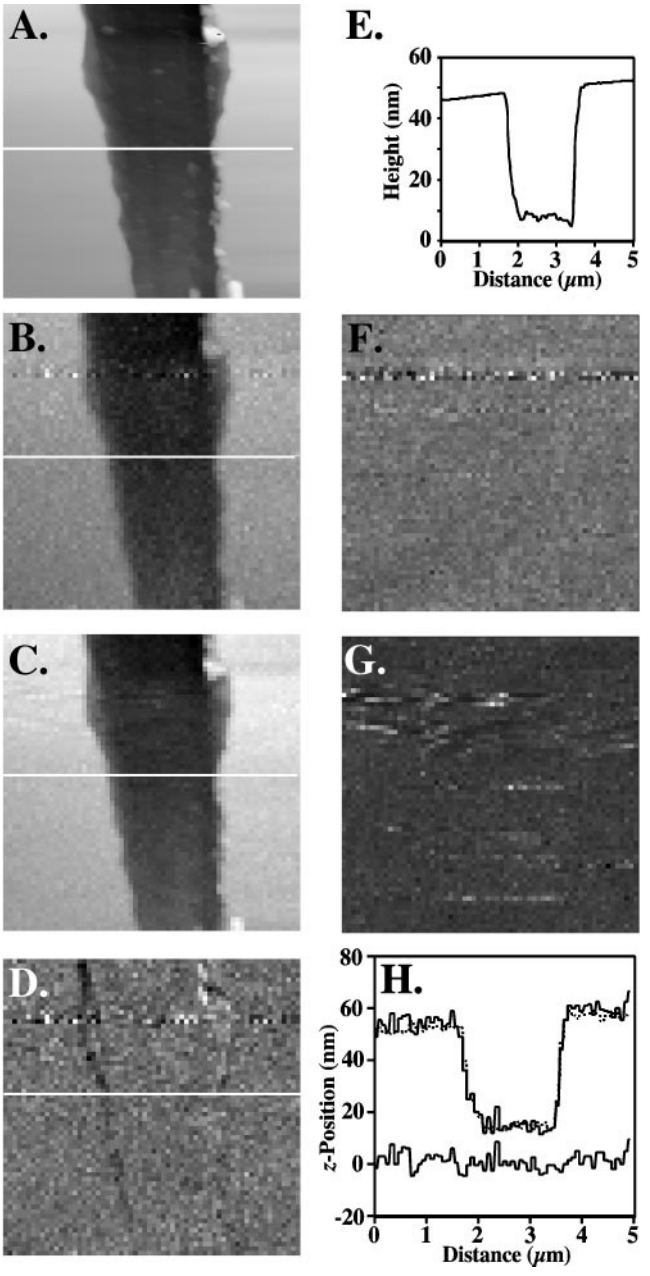

FIGURE 3 D–D mapping of a sample of constant charge and varying topography (mechanically roughened mica; 5 × 5 μm image size; $h > \lambda$). (*A*) Contact mode AFM image of the sample and (*E*) line profile showing the topography. (*B*) FV isoforce surface of the area in (*A*) collected in a low salt solution and (*F*) the corresponding Debye length map. (*C*) FV isoforce surface collected in a high-salt solution and (*G*) the corresponding Debye length map. (*D*) D–D map made by subtracting the isoforce surface in (*C*) from the isoforce surface in (*B*) and dividing by the difference in Debye lengths (Eq. 8). The linear gray scale in the D–D map corresponds to the range of $\ln(\sigma_1/\sigma_2)$. (*H*) Line profiles of the FV isoforce surfaces (low-salt, *upper solid line*; high-salt, *gray line*) and the corresponding difference in *z*-positions used to construct the D–D map (*lower solid line*). The D–D map has no contrast because the isosurfaces contain only sample height information and no electrostatic contributions. This demonstrates that D–D maps are independent of topography for samples where $h > \lambda$. The linear gray scale range corresponds to (*A*) 100 nm, (*B*) 100 nm, (*C*) 100 nm, (*D*) −1.0–1.0, (*F*) 0–30 nm, (*G*) 0–20 nm.

larger at the lower salt concentration, which gives rise to an edge artifact.

The second sample of constant charge density and varying topography was prepared by adsorbing DPPS to a polylysine-coated mica surface. Under appropriate conditions this results in stacked lipid bilayers, with topographic steps of ~6 nm (Fig. 4, *A* and *E*) and a constant negative charge at neutral pH. The stacked DPPS bilayers correspond to the $h \simeq \lambda$ case. As in the rough mica example, the force volumes of the DPPS bilayers with $F_{tr} = 5$ nm result in isoforce surfaces containing topographic information (Fig. 4, *B* and *C*), flat Debye length maps (Fig. 4, *F* and *G*) with Debye lengths of 6 ± 2 and 2 ± 0.6 nm for the low and high salt conditions, and a flat D–D map (Fig. 4, *D* and *H*) indicating a uniform surface charge density. While not as pronounced as in the rough mica D–D map, there are again some edge effects.

D–D map of a surface with varying charge density and varying topography

To test the D–D mapping on surfaces with variations in charge density and topography we made supported DPPC bilayer patches on mica substrates. The bilayer has a step height of ~6 nm (Fig. 5, *A* and *E*). DPPC is zwitterionic, but at neutral pH it has a small negative charge. Similarly, the mica substrate and the silicon nitride tip are negatively charged at this pH.

Force volumes were collected over the DPPC bilayers on mica in solutions of three different salt concentrations. Contact-mode images of the sample area before (not shown) and after (Fig. 5 *A*) the FV images verify the lipids were not damaged during the imaging (although some lateral drift occurred). Force mapping over DPPC bilayer membranes on mica in different NaCl concentrations with $F_{tr} = 7$ nm reveal contrast inversion with changes in salt concentration (Fig. 5, *B–D*). Force curves from each volume produced low contrast Debye length maps (Fig. 5, *G–I*) with Debye lengths of 15 ± 1.7, 13 ± 2, and 5 ± 2 nm for the three different salt solutions. Subtracting the high-salt isoforce surface (Fig. 5 *D*) from the low-salt isoforce surface (Fig. 5 *B*) yields a relative charge density map (Fig. 5 *E*) whose contrast is inverted relative to the topographic image (Fig. 5 *A*). Line profiles of the low-salt, high-salt, and D–D maps are shown in Fig. 5 *J*.

At a low salt concentration, the electrostatic double layers of the tip and mica extend relatively far from their surfaces. Because the DPPC bilayer has a very low charge density, it has a very weak double layer. Therefore, according to Eq. 1, in solutions with long Debye lengths the double layers of the tip and mica substrate will overlap and produce a repulsive force at a distance much greater than the distance at which the tip's double layer interacts with the DPPC and produces a similar force. This is the basis for the contrast inversion in the isoforce surface measured in low salt relative to the topography (Fig. 5 *B* versus 5 *A*). At a high salt concentration, the Debye length is short, and the double

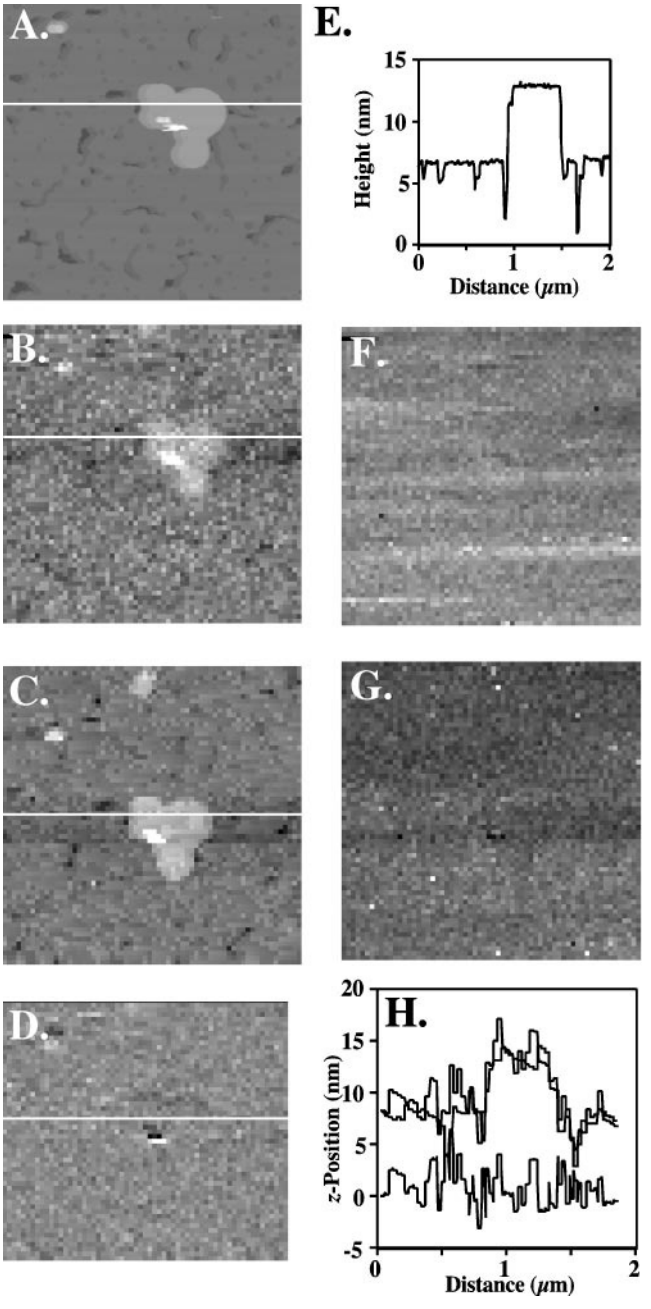

FIGURE 4 D–D mapping of a sample of constant charge and varying topography (stacked DPPS bilayers; 2×2 μm image size; $h \simeq \lambda$). (*A*) Contact mode AFM image of the sample and (*E*) line profile showing the topography. (*B*) FV isoforce surface of the area in (*A*) collected in a low-salt solution and (*F*) the corresponding Debye length map. (*C*) FV isoforce surface collected in a high-salt solution and (*G*) the corresponding Debye length map. (*D*) D–D map made by subtracting the isoforce surface in (*C*) from the isoforce surface in (*B*) and dividing by the difference in Debye lengths (Eq. 8). The linear gray scale in the D–D map corresponds to the range of $\ln(\sigma_1/\sigma_2)$. (*H*) Line profiles of the FV isoforce surfaces (low-salt, *upper solid line*; high-salt, *gray line*) and the corresponding difference in *z*-positions used to construct the D–D map (*lower solid line*). Again, the D–D map has no contrast because the isosurfaces contain only sample height information and no electrostatic contributions. This demonstrates that D–D maps are independent of topography for samples with $h = \lambda$. The linear gray scale range corresponds to (*A*) 20 nm, (*B*) 20 nm, (*C*) 20 nm, (*D*) −2.5–2.5, (*F*) 0–30 nm, (*G*) 0–10 nm.

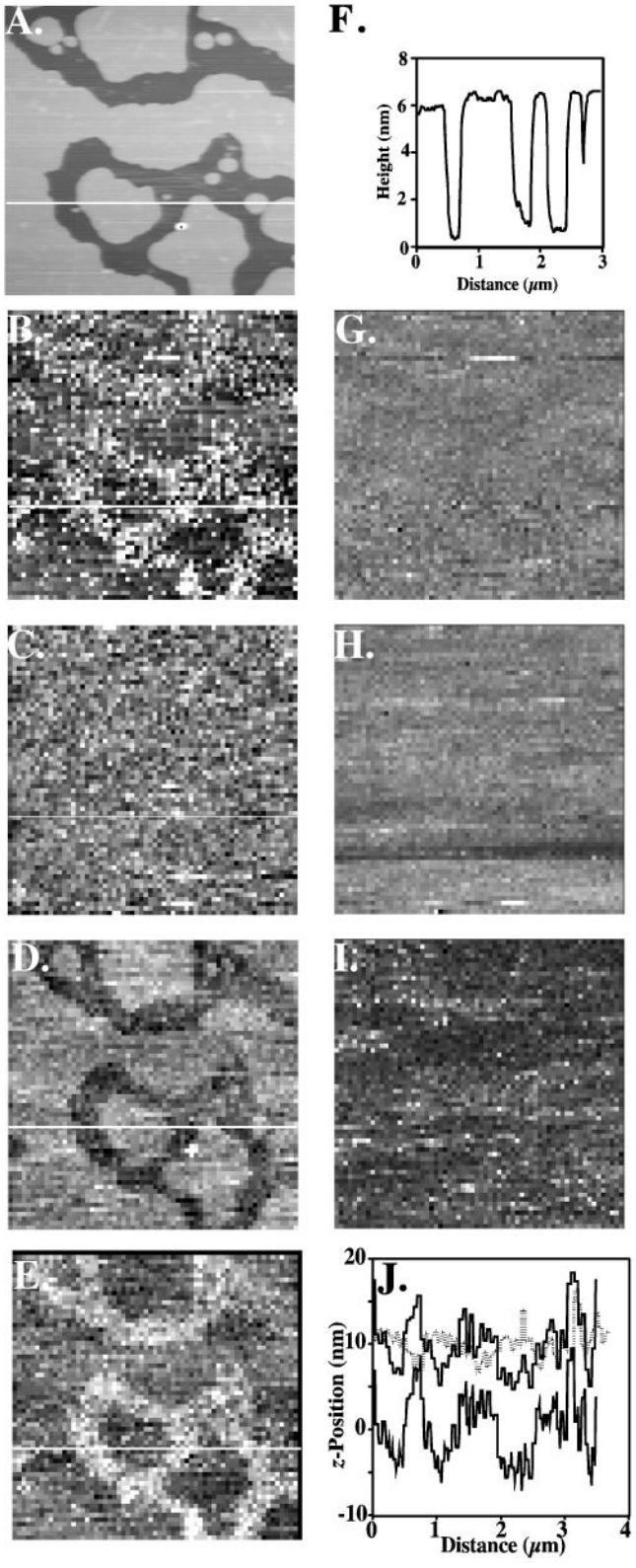

FIGURE 5 D–D mapping of a sample with varying charge and varying topography (patches of DPPC on mica; 4 × 4 μm scan size). (*A*) Contact mode AFM image of the sample and (*E*) line profile showing the topography. (*B*) FV isoforce surface of the area in (*A*) taken in a low-salt solution and (*G*) the corresponding Debye length map. (*C*) FV isoforce surface collected in an intermediate salt solution and (*H*) the corresponding Debye length map. (*D*) FV isoforce surface collected in a high-salt solution and (*I*) the corresponding Debye length map. (*E*) D–D map made by subtracting the isoforce surface in (*D*) from the isoforce surface in (*B*) and dividing by the difference in Debye lengths (Eq. 8). The linear gray scale in the D–D map corresponds to the range of $\ln(\sigma_1/\sigma_2)$. The values in the map are relative to the value of a randomly selected DPPC pixel. (*J*) Line profiles of the FV isoforce surfaces (low-salt, *upper solid line*; high-salt, *gray line*) and the corresponding difference in *z*-positions used to construct the D–D map (*lower solid line*). The contrast in the FV images is dependent on salt concentration and undergoes an inversion as salt is added to the solution. The D–D map's contrast is inverted relative to the topographic contact map, and this demonstrates that D–D maps show variation of surface charge density independent of topography. The linear gray scale range corresponds to (*A*) 10 nm, (*B*) 20 nm, (*C*) 20 nm, (*D*) 20 nm, (*E*) −1.0–1.0, (*G*) 0–25 nm, (*H*) 0–25 nm, (*I*) 0–15 nm.

layers of the tip and the mica are very close to their surfaces. The double layers will overlap and produce a repulsive force, but at a distance comparable to the tip-DPPC interaction distance. Therefore, at high salt concentrations, an isoforce surface over the DPPC-mica sample will follow the topography of the sample more closely than at the low salt concentration (Fig. 5 *D*). At an intermediate salt concentration, the double layers of tip and mica will overlap at a tip-mica separation of ~6 nm, producing a low contrast isoforce surface (Fig. 5 *C*).

The isoforce surfaces combine physical topography with electrostatic effects (Müller and Engel, 1997). By subtracting the high-salt surface (Fig. 5 *D*) from the low-salt surface (Fig. 5 *B*), we can remove the topographic information, leaving a surface whose height differences correspond to the natural log of the surface charge density ratio (Figs. 1 *E* and 5 *E*). In the D–D map lighter areas have a higher relative surface charge density.

Features in the low-salt images appear slightly blurred compared to the high-salt images (Figs. 3–6). This is probably due to the lower charge screening ability of the low salt solution. In short Debye length solutions, the tip will deflect due to charges directly under it, whereas in a long Debye length environment, the AFM tip will respond to more distant charges as well as those immediately beneath it. The final effect will be a broadening in x and y of surface features in the low-salt images and an outline around the features in the D–D map. Again, while the outline could be the result of electrostatic edge effects, it most likely is an artifact of the subtraction process.

D–D mapping of bacteriorhodopsin

To determine the relative surface charge density of a biological sample, we applied the D–D mapping method to BR membranes to adsorbed mica substrates. BR membranes have a height of ~6 nm (Fig. 6, *A* and *E*). Both BR membranes and mica are negatively charged. Previous studies using the AFM (Butt, 1992) and other methods (Alexiev et al., 1994; Jonas et al., 1990; Renthal and Cha, 1984) have reported the surface charge density of BR membranes to be within 0.22–1.9 e^-/nm^2. Mica has a similar broad range of reported values of surface charge density between 0.02 and

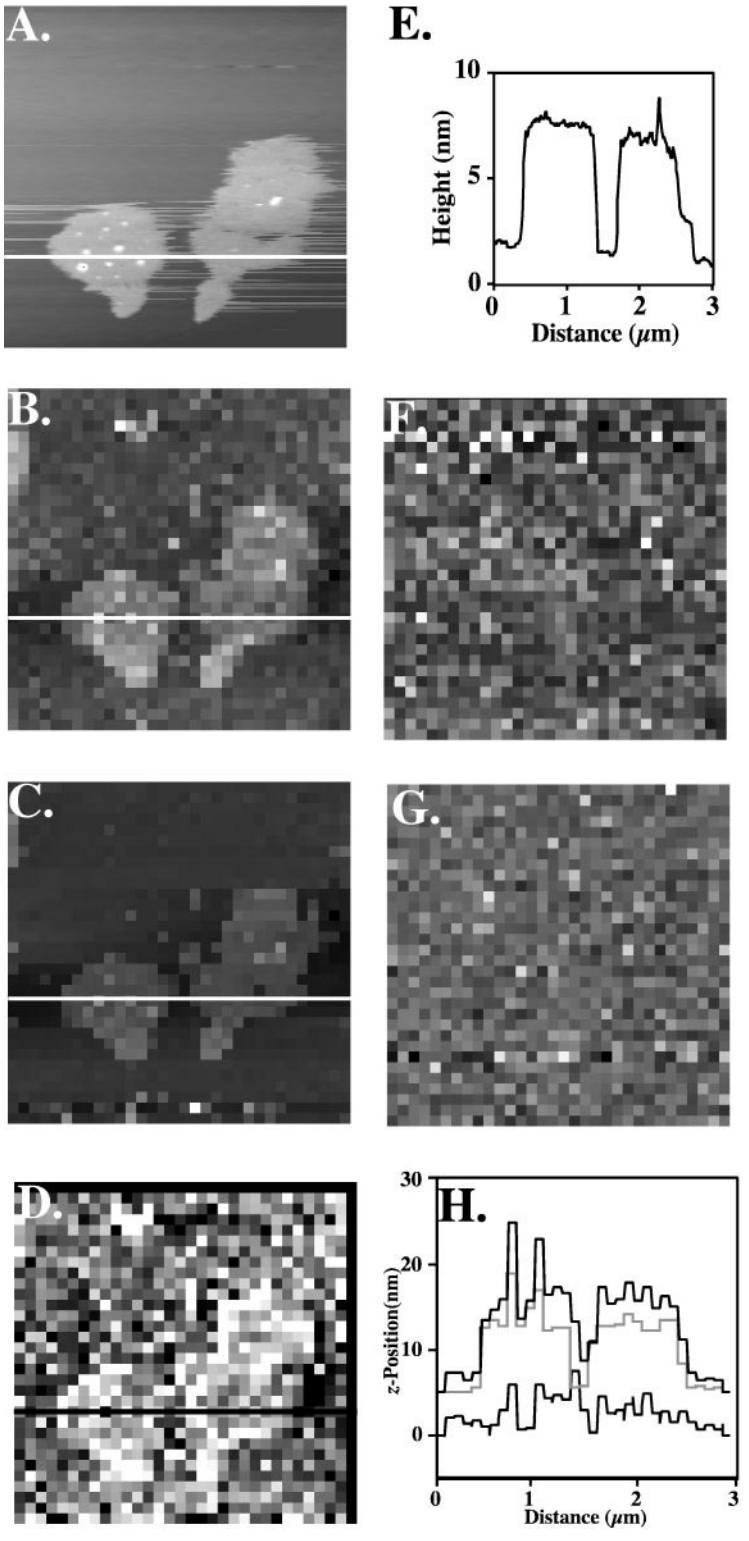

FIGURE 6 D–D mapping of bacteriorhodopsin membranes on mica (3×3 μm image size). (*A*) Contact mode AFM image of the sample and (*E*) line profile showing the topography. (*B*) FV isoforce surface of the area in (*A*) taken in a low-salt solution and (*F*) the corresponding Debye length map. (*C*) FV isoforce surface collected in a high-salt solution and (*G*) the corresponding Debye length map. (*D*) D–D map made by subtracting isoforce surface in (*C*) from the isoforce surface in (*B*) and dividing by the difference in Debye lengths (Eq. 8). The linear gray scale in the D–D map corresponds to the range of $\ln(\sigma_1/\sigma_2)$. The values in the map are relative to the value of a randomly selected mica pixel. (*H*) Line profiles of the FV isoforce surfaces (low-salt, *upper solid line*; high-salt, *gray line*) and the corresponding difference in *z*-positions used to construct the D–D map (*lower solid line*). The D–D map demonstrates that the surface charge density of BR membranes is $\sim 3\times$ greater than that of mica. The linear gray scale range corresponds to (*A*) 10 nm, (*B*) 25 nm, (*C*) 25 nm, (*D*) -1.0–2.5, (*F*) 0–20 nm, (*G*) 0–20 nm.

0.5 e^-/nm^2 (Pashley, 1981; Israelachvili and Adams, 1977). Therefore, the mica surface charge densities are expected to be less than the value for BR membranes.

We collected FVs over BR membranes in two different NaCl concentrations to a trigger threshold of 15 nm. The isoforce surfaces reveal the underlying topography of the sample without the tip contacting the sample (Fig. 6, *B* and *C*). Fitting the force curves from each FV yields flat Debye length maps (Fig. 6, *F* and *G*) with Debye lengths of 11 ± 2 and 7 ± 2 nm. Subtracting the high-salt isoforce surface (Fig. 6 *C*) from the low-salt isoforce surface (Fig. 6 *B*) produces a D–D map of the surface (Fig. 6 *D*) that shows that the BR membranes are approximately three times as charged as the mica. This is consistent with previously

reported AFM measurements (Butt, 1992; Müller and Engel, 1997).

Limitations of D–D Mapping

Spatial resolution is Debye length-dependent because, at low salt concentrations, the tip will feel forces from distant charges as well as from those directly under it. Furthermore, because the counterion concentration decays exponentially in the direction normal to the surface and is constant parallel to the surface, the contribution of distant charges to the detected force will vary as the tip approaches the sample. Ideally, these measurements should be made at salt concentrations with Debye lengths that are less than the dimensions of an *x-y* pixel. Spatial resolution is also tip-dependent since the double layer force acts over an area defined by the tip size.

One limit to the charge sensitivity of the approach described here can be estimated from the radius and surface charge density of the tip, the cantilever spring constant (K_c), and the thermally induced oscillations of the cantilever. From Eq. 1, the following condition must be met to detect double layer forces resulting from surface charges at a tip-sample separation of $D = \lambda$:

$$\sigma_S > \frac{\sqrt{K_c}}{(R\lambda)\sigma_R}\left(\frac{e\epsilon\sqrt{2k_BT}}{4\pi}\right) \quad (9)$$

where T is the absolute temperature of the system, k_B is Boltzmann's constant, and the other symbols retain their previous definitions. For a typical silicon nitride cantilever with a spring constant of 0.01 N/m, a tip of radius 15 nm and surface charge density of 0.032 C/m^2 (0.2 e$^-$/nm^2) (Butt, 1991a), in a electrolyte solution with a Debye length of 10 nm at room temperature, σ_s must be $>1.8 \times 10^{-3}$ e$^-$/nm^2 in order to obtain a signal-to-noise ratio greater than one. In practice it is at present not possible to approach this limit, in part because other noise sources are much larger than thermal noise (over the time scale of the experiments). To detect the small forces generated by low surface charge densities, a highly charged tip coupled with a large Debye length and a flexible cantilever is favorable in terms of increasing the signal-to-noise ratio. However, increasing the Debye length comes at the price of reduced lateral charge resolution. A tip with a large radius is also helpful; however, a wide tip will also lower the *x-y* resolution of the D–D map.

D–D mapping is based on Gouy-Chapman theory, which assumes the potential at the surface-electrolyte interface is much less than k_BT. At room temperature this corresponds to surface potentials of <25 mV. For surfaces meeting this condition, the D–D map is a quantitative map of relative surface charge density and, by application of Gouy-Chapman theory, relative surface potential. For other surfaces, the D–D map, while not quantitative, can provide useful information such as charge density differences and distributions across a surface.

The approach described here is based on using force volumes to construct isoforce surfaces. This can be time-consuming and each of the volumes described in this paper was acquired in $\sim$1 h. This time can increase significantly as the density of curves is increased to achieve higher *x-y*-resolution. High-resolution isoforce surfaces can, in principle, be made in "contact" mode imaging by adjusting the setpoint to F_{tr}. (Senden et al., 1994; Manne et al., 1994). However, in practice the cantilever and piezo drift appreciably (more than several nm) during the course of a scan, resulting in time-dependent changes in force or topography. This is not a significant problem with the force volume approach, in which the drift only needs to be small on the time scale of two force curves ($\sim$1 s). If the technical problem of collecting driftless isoforce surfaces in "contact" mode is solved, the analysis can proceed as described above.

Lastly, it should be noted that not all biological systems can withstand even small changes in ionic strength. Using non-ionic solutes to make the solution isotonic may be a way to address this problem. However, in general, D–D mapping requires only a detectable difference in Debye lengths, not necessarily a large difference, to produce quantitative relative surface charge density maps.

CONCLUSIONS

Local electrostatic properties have a profound impact on the structure and function of biological systems. We have developed an experimental approach, called D–D mapping, which uses an AFM to produce maps of relative surface charge density of samples in aqueous solutions. D–D mapping has the advantages of being independent of tip-sample contact point, cantilever spring constant, tip radius, and tip surface charge density. Also, damage to the sample and contamination of the tip are minimized in the D–D mapping approach. Uniform D–D maps of a mechanically roughened mica substrate and stacked DPPS bilayers show the maps contain no topographic information, and D–D maps of DPPC bilayers on mica demonstrate that the contrast is due to charge density differences and is uncoupled from topography. A D–D map of BR membranes on mica shows BR has a higher surface charge density than mica. These results present a mode of high-resolution imaging in which the contrast is based on surface electrostatics of biological material.

This work was supported in part by a grant from the Council for Tobacco Research (to J.H.H.). William F. Heinz was supported in part by National Institutes of Health Predoctoral Training Grant T32 GM-08043 through the Intercampus Program in Molecular Biophysics.

REFERENCES

Alexiev, U., T. Marti, M. P. Heyn, H. G. Khorana, and P. Scherrer. 1994. Surface charge of bacteriorhodopsin detected with covalently bound pH

indicators at selected extracellular and cytoplasmic sites. *Biochemistry.* 33:298–306.

Barthel, D., O. Zschoernig, K. Lange, R. Lenk, and K. Arnold. 1988. Interaction of electrically charged drug molecules with phospholipid membranes. *Biochim. Biophys. Acta.* 945:361–366.

Biggs, S., and A. D. Proud. 1997. Forces between silica surfaces in aqueous solutions of a weak polyelectrolyte. *Langmuir.* 13:7202–7210.

Binnig, G., C. F. Quate, and C. Gerber. 1986. Atomic force microscope. *Phys. Rev. Lett.* 56:930–933.

Butt, H.-J. 1991a. Measuring electrostatic, van der Waals, and hydration forces in electrolyte solution with an atomic force microscope. *Biophys. J.* 60:1438–1444.

Butt, H.-J. 1991b. Electrostatic interactions in atomic force microscopy. *Biophys. J.* 60:777–785.

Butt, H.-J. 1992. Measuring local surface charge densities in electrolyte solutions with a scanning force microscope. *Biophys. J.* 63:578–582.

Castle, J. D., and W. L. Hubbell. 1976. Estimation of membrane surface potential and charge density from the phase equilibrium of a paramagnetic amphiphile. *Biochemistry.* 15:4818–4831.

Cevc, G. 1990. Membrane electrostatics. *Biochim. Biophys. Acta.* 1031: 311–382.

D'Costa, N. P., and J. H. Hoh. 1995. Calibration of optical lever sensitivity for atomic force microscopy. *Rev. Sci. Instrum.* 66:5096–5097.

Danon, D., L. Goldstein, Y. Marikovsky, and E. Skutelsky. 1972. Use of cationized ferritin as a label of negative charges on cell surfaces. *J. Ultrastruct. Res.* 38:500–510.

Ducker, W. A., T. J. Senden, and R. M. Pashley. 1991. Direct measurement of colloidal forces using an atomic force microscope. *Nature.* 353: 239–241.

Ducker, W. A., T. J. Senden, and R. M. Pashley. 1992. Measurement of forces in liquids using a force microscope. *Langmuir.* 8:1831–1836.

Ehrenberg, B. 1986. Spectroscopic methods for the determination of membrane surface charge density. *Methods Enzymol.* 127:678–696.

Fang, Y., and J. Yang. 1997. The growth of bilayer defects and the induction of interdigitated domains in the lipid-loss process of supported phospholipid bilayers. *Biochim. Biophys. Acta.* 1324:309–319.

Hansma, P. K., B. Drake, O. Marti, S. A. C. Gould, and C. B. Prater. 1989. The scanning ion-conductance microscope. *Science.* 243:641–643.

Heinz, W. F., and J. H. Hoh. 1997. Relative surface charge density maps of bacteriorhodopsin membranes determined from the interaction force field. *Programs and Abstracts, Biophysical Journal*. 72:403*a*.

Hillier, A. C., S. Kim, and A. J. Bard. 1996. Measurement of double-layer forces at the electrode/electrolyte interface using the atomic force microscope: potential and anion dependent interactions. *J. Phys. Chem.* 100:18808–18817.

Israelachvili, J. N. 1992. Intermolecular and surface forces. Academic Press, New York. 450 pp.

Israelachvili, J., and G. Adams. 1977. Measurement of forces between two mica surfaces in aqueous electrolyte solutions in the range 0–100 nm. *J. Chem. Soc., Faraday Trans. I.* 74:975–1000.

Jaffe, L. F., and R. Nuccitelli. 1974. An ultrasensitive vibrating probe for measuring steady extracellular currents. *J Cell Biol.* 63:614–628.

Johnson, C. A., and A. M. Lenhoff. 1996. Adsorption of charged latex particles on mica studied by atomic force microscopy. *J. Colloid Interface Sci.* 179:587–599.

Jonas, R., Y. Koutalos, and T. G. Ebrey. 1990. Purple membrane: surface charge density and the multiple effect of pH and cations. *Photochem. Photobiol.* 52:1163–1177.

Larson, I., C. J. Drummond, D. Y. C. Chan, and F. Grieser. 1997. Direct force measurements between silica and alumina. *Langmuir*. 13: 2109–2112.

Manne, S., J. P. Cleveland, H. E. Gaub, G. D. Stucky, and P. K. Hansma. 1994. Direct visualization of surfactant hemimicelles by force microscopy of the electrical double layer. *Langmuir.* 10:4409–4413.

McLaughlin, S. 1989. The electrostatic properties of membranes. *Annu. Rev. Biophys. Biophys. Chem.* 18:113–136.

Müller, D. J., and A. Engel. 1997. The height of biomolecules measured with the atomic force microscope depends on electrostatic interactions. *Biophys. J.* 73:1633–1644.

Pashley, R. M. 1981. DLVO and hydration forces between mica surfaces in Li, Na, K and Cs electrolyte solutions: a correlation of double-layer and hydration forces with surface cation exchange properties. *J. Colloid Interface Sci.* 83:531–546.

Raiteri, R., M. Gratarola, and H.-J. Butt. 1996a. Measuring electrostatic double-layer forces at high surface potentials with the atomic force microscope. *J. Phys. Chem.* 100:16700–16705.

Raiteri, R., S. Martinoia, and M. Grattarola. 1996b. pH-dependent charge density at the insulator-electrolyte interface probed by a scanning force microscope. *Biosensors and Bioelectronics.* 11:1009–1017.

Renthal, R., and C. H. Cha. 1984. Charge asymmetry of the purple membrane measured by uranyl quenching of dansyl fluorescence. *Biophys J.* 45:1001–1006.

Rotsch, C., and M. Radmacher. 1997. Mapping local electrostatic forces with the atomic force microscope. *Langmuir.* 13:2825–2832.

Senden, T. J., C. J. Drummond, and P. Kekicheff. 1994. Atomic force microscopy: imaging electrical double layer interactions. *Langmuir.* 10:358–362.

Tamm, L. K., and H. M. McConnell. 1985. Supported phospholipid bilayers. *Biophys J.* 47:105–113.